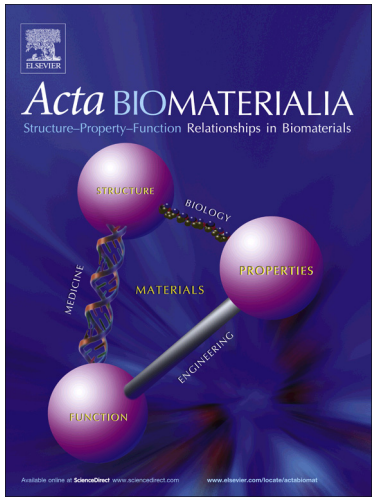


# Substrate topography: A valuable *in vitro* tool, but a clinical red herring for *in vivo* tenogenesis

Andrew English, Ayesha Azeem, Kyriakos Spanoudes, Eleanor Jones, Bhawana Tripathi, Nandita Basu, Karrina McNamara, Syed A.M. Tofail, Niall Rooney, Graham Riley, Alan O'Riordan, Graham Cross, Dietmar Hutmacher, Manus Biggs, Abhay Pandit, Dimitrios I. Zeugolis

PII: S1742-7061(15)30079-9
DOI: http://dx.doi.org/10.1016/j.actbio.2015.08.035
Reference: ACTBIO 3849

To appear in: *Acta Biomaterialia*

Received Date: 29 March 2015
Revised Date: 22 August 2015
Accepted Date: 25 August 2015

Please cite this article as: English, A., Azeem, A., Spanoudes, K., Jones, E., Tripathi, B., Basu, N., McNamara, K., Tofail, S.A.M., Rooney, N., Riley, G., O'Riordan, A., Cross, G., Hutmacher, D., Biggs, M., Pandit, A., Zeugolis, D.I., Substrate topography: A valuable *in vitro* tool, but a clinical red herring for *in vivo* tenogenesis, *Acta Biomaterialia* (2015), doi: http://dx.doi.org/10.1016/j.actbio.2015.08.035

**Title**

Substrate topography: A valuable *in vitro* tool, but a clinical red herring for *in vivo* tenogenesis

**Authors**

Andrew English [1, 2, 3], Ayesha Azeem [1, 2, 3], Kyriakos Spanoudes [1, 2, 3], Eleanor Jones [4], Bhawana Tripathi [5], Nandita Basu [5], Karrina McNamara [6], Syed A.M. Tofail [6], Niall Rooney [7], Graham Riley [4], Alan O'Riordan [8], Graham Cross [5], Dietmar Hutmacher [9], Manus Biggs [2, 3], Abhay Pandit [2, 3] and Dimitrios I. Zeugolis [1, 2, 3, *]

**Affiliations**

1. Regenerative, Modular & Developmental Engineering Laboratory (REMODEL), Biosciences Research Building (BRB), National University of Ireland Galway (NUI Galway), Galway, Ireland

2. Network of Excellence for Functional Biomaterials (NFB), BRB, NUI Galway, Galway, Ireland

3. Centre for Research in Medical Devices (CÚRAM), BRB, NUI Galway, Galway, Ireland

4. School of Biological Sciences, University of East Anglia, Norwich, UK

5. Centre for Research on Adaptive Nanostructures and Nanodevices (CRANN), Trinity College Dublin, Dublin, Ireland

6. Materials and Surface Science Institute (MSSI), Department of Physics and Energy, University of Limerick, Limerick, Ireland

7. Proxy Biomedical, Galway, Ireland

8. Tyndall National Institute, Cork, Ireland

9. Institute of Health & Biomedical Innovation, Queensland University of Technology, Australia

***Correspondence Author:**

Dr Dimitrios Zeugolis, REMODEL, NFB, CURAM, NUI Galway, Galway, Ireland; E-mail: dimitrios.zeugolis@nuigalway.ie; Office: +353-(0)-9149-3166; Fax: +353-(0)-9156-3991

**Abstract**

Controlling the cell-substrate interactions at the bio-interface is becoming an inherent element in the design of implantable devices. Modulation of cellular adhesion *in vitro*, through topographical cues, is a well-documented process that offers control over subsequent cellular functions. However, it is still unclear whether surface topography can be translated into a clinically functional response *in vivo* at the tissue / device interface. Herein, we demonstrated that anisotropic substrates with a groove depth of ~317 nm and ~1,988 nm promoted human tenocyte alignment parallel to the underlying topography *in vitro*. However, the rigid poly(lactic-co-glycolic acid) substrates used in this study upregulated the expression of chondrogenic and osteogenic genes, indicating possible tenocyte trans-differentiation. Of significant importance is that none of the topographies assessed (~37 nm, ~317 nm and ~1,988 nm groove depth) induced extracellular matrix orientation parallel to the substrate orientation in a rat patellar tendon model. These data indicate that two-dimensional imprinting technologies are useful tools for *in vitro* cell phenotype maintenance, rather than for organised neotissue formation *in vivo*, should multifactorial approaches that consider both surface topography and substrate rigidity be established.

**Keywords**

Tendon; Surface topography; Substrate stiffness; Lithography; Tenocyte morphology; Tenocyte Phenotype; Tenocyte trans-differentiation; Tissue regeneration

## 1. Introduction

Given the poor inherent regeneration capability of tendons, largely attributed to low vascularity and low activity cellular content, intervention strategies should be developed to promote functional tendon repair and regeneration. Given that tissue graft based therapies have failed to restore native tendon function, it is anticipated that the tissue-engineering arpeggio (scaffolds, cells, biologics alone or in combination) would provide a functional therapy in the years to come [1-13].

Biomaterials' design and development is coming ever closer to mimicking native extracellular matrix (ECM) assemblies, as advancements in engineering have allowed development of two- and three- dimensional substrates with precise mechano-architectural and chemical properties. Indeed, current biomaterial fabrication technologies not only achieve structural support, but also maintain permanently differentiated cell phenotype and/or direct lineage commitment of stem cells. For example, topographical features have been shown to maintain Oct4 expression in human embryonic stem cell culture, even in the absence of basic fibroblast growth factor supplementation [14]; topographical cues alone [15, 16] or in combination with neurotrophic signals [17] have also been shown to enhance contact guidance and neuronal differentiation of human neural stem cells *in vitro*. Topographical cues have been shown to enhance myogenic differentiation and maturation of myoblasts [18] and to induce myogenic commitment of human mesenchymal stem cells *in vitro* [19]. Surface topography alone [20] or in combination with substrate rigidity [21] have been shown to control mesenchymal stem cell lineage commitment. Recently, multi-scale patterned substrates have been shown to control adhesion and differentiation of human mesenchymal stem cells [22] and topographical features combined with hyaluronic acid have been shown to enhance chondrogenic differentiation of dental pulp stem cells [23]. Furthermore, two-dimensional and three-dimensional patterning technologies have been shown to enhance osteo-induction of stem cells [24], whilst proliferation and osteogenic differentiation of human mesenchymal stem cells have been shown to be dependent on the size of the underlying structures [25]. However, optimal feature geometries and conformations (e.g. grooves, pillars) and dimensionality (e.g. nano, micro) of such topographical

features remain elusive, despite significant scientific achievements and technological innovations in fabrication processes and *in vitro* analysis.

To date, two- and three- dimensional scaffold fabrication technologies (e.g. electro-spinning [26-31], fibre extrusion [32-35], isoelectric focusing [36, 37] and imprinting [38-40]) have been at the forefront of scientific and technological research and innovation to recapitulate native tendon extracellular matrix (ECM) supramolecular assemblies. Although fibrous constructs (e.g. electro-spun polymeric fibres, extruded collagen fibres and isoelectrically focused collagen fibres) have been shown to maintain tenocyte phenotype and to differentiate stem cells towards tenogenic lineage *in vitro* and to induce acceptable regeneration in preclinical models, none of these technologies offers precise control over the spatial distribution of the fibres. Imprinting technologies, on the other hand, have demonstrated a diverse effect on a range of permanently differentiated and stem cell functions, including adhesion, orientation, secretome expression and lineage commitment [41-48] and offer significantly greater control over feature dimension and spacing. Specifically to tendon repair, such technologies have been shown to maintain tenocyte phenotype [38]; to promote aligned tendon-specific ECM deposition [39]; and to differentiate stem cells towards tenogenic lineage [40]. Despite these advancements, a comprehensive study on the influence of surface features with respect to the modulation of tenocyte phenotype *in vitro* through anisotropic nano- to micron- scale topographies and on tissue response *in vivo* has yet to be elucidated. Thus, in the present study, we employed imprint lithography to create anisotropically grooved substrates with constant width and spacing and varying depth, as opposed to isotropic topography, to study tenocyte function *in vitro* and the host tissue response *in vivo*.

## 2. Materials and Methods

### 2.1. Anisotropic substrate fabrication

The process of substrate fabrication has been described previously [49]. Briefly, Si master moulds with anisotropic topographies were fabricated via a photolithography process, followed by reactive ion etching (RIE). 1.5 x 1.5 $cm^2$ regions were patterned with lines / gratings of 2,101.78 ± 35.21 nm and 1,911.42 ± 37.50 nm widths respectively, and variable groove depths (37.48 ± 3.4 nm, 317.29 ± 7.05 nm and 1,988.2 ± 195.3 nm). Silicon wafers (3.0 x 3.0 $cm^2$) were spin-coated with a positive photoresist (S1813 PR, Shipley) and then exposed using OAI Mask Aligner (Model MBA800). Following photoresist development, the master mould was etched by RIE (Oxford ICP etcher) using CHF3 + SF6 ionised gas. The moulds were silanised with 5 mM octadecyltrichlorosilane (OTS, Sigma Aldrich, Ireland) solution to facilitate imprint release. A thermal imprinting process was used to transfer the master pattern into a 2.0 x 2.0 $cm^2$ PLGA substrate (85:15, Sigma Aldrich, Ireland) using a Specac Hydraulic Press (15 T & 25 T) at 120 °C and a pressure of 5 MPa, for 5 min. The imprinted gratings on polymer were subsequently analysed by SEM and AFM. Non-imprinted PLGA substrates were used as isotropic control substrates.

### 2.2. Surface chemical analysis

X-ray photoelectron spectroscopy (XPS) analysis was performed in a Kratos AXIS 165 X-ray photoelectron spectrometer using monochromatic Al K$\alpha$ radiation of energy 1486.6 eV and operated at beam voltage of 15 kV and beam current of 10 mA. High-resolution spectra of O 1s, C 1s and Si 2p were taken at fixed pass energy of 20 eV. Construction and peak fitting of synthetic peaks in narrow region spectra used a Shirely type background and the synthetic peaks were of a mixed Gaussian-Lorenzian type. Relative sensitivity factors used are from CasaXPS library containing Scofield cross-sections. Binding energies were determined using C 1s peak at 284.8 eV as charge reference.

### 2.3. Human tenocyte culture

Human primary tenocytes (positive for tenomodulin, scleraxis and tenascin C; Cambridge Biosciences, UK) were cultured in Dulbecco's Modified Eagle's Medium (DMEM) supplemented 10 % foetal bovine serum and 1 % penicillin/streptomycin (all Sigma Aldrich, Ireland). Cells were maintained at 37 °C and 5 % carbon dioxide, with the media being changed every 3 days. Tenocytes were sub-cultured when 80 % confluency was reached. Tenocytes were detached from the culture flask with trypsin-EDTA solution (Sigma Aldrich, Ireland) and then seeded on the imprinted and isotropic substrates in 12-well (Ibidi®, Germany) and 8-well (Lab-Tek™, Thermo Scientific, UK) chamber slides at a cell density of 20,000 cells per 1 $cm^2$ for morphometric, viability, proliferation and metabolic activity analyses and 25,000 cells per 1 $cm^2$ for gene expression analysis (sufficient quality and quantity of RNA was obtained at this density), respectively. All *in vitro* experiments were conducted for 1, 5, and 10 days and cells at passage 3 were used.

### 2.4. Human tenocyte morphometric analysis

Immunofluorescent images were used to evaluate cell morphology and alignment. At the end of culture points, the substrates were washed three times with Hanks Balanced Salt Solution (HBSS, Sigma Aldrich, Ireland) and the cells were fixed with 4 % paraformaldehyde (Sigma Aldrich, Ireland) for 15 min at room temperature (RT). The cells were washed again in HBSS three times and then permeabilised with 0.2 % Triton X (Sigma Aldrich, Ireland) for 5 min. The cells were then exposed to 4',6-diamidino-2-phenylindole (DAPI, Molecular Probes, Ireland) in phosphate buffer saline (PBS) for 5 min, washed with HBSS and then exposed to rhodamine conjugated phalloidin (Molecular Probes, Ireland) in PBS for 1 h. Images were captured with a 10X objective, using an inverted BX51 Olympus fluorescence microscope (Olympus, Japan).

Immunofluorescent micrographs of tenocytes were quantitatively analysed using ImageJ software (NIH). Briefly, images were converted to 8-bit grey scale and threshold to distinguish cellular outlines from the non-cellular background signal; the program detected cells on the basis of contrast

and fitted the cellular outlines to equivalent ellipses. The following cell shape characteristics were measured for each fitted ellipse: major axis, minor axis, aspect ratio (major axis / minor axis), perimeter, area, and orientation angle with respect to the direction of grooves. Cellular orientation / alignment was determined by the angle between the major axis of the cell and the groove direction. The angle for each cell was converted such that 0 ° represented cell orientation along the direction of the grooves and 90 ° represented a perpendicular orientation, with respect to the direction of the grooves. Cells within 10 ° of the groove direction were considered aligned. Cell morphology was quantified using aspect ratio (major axis/minor axis). Aspect ratio was used to evaluate cellular elongation, with a higher aspect ratio indicating increased elongation. Cells that overlapped or aggregated together or wherever boundaries of contacting cells could not be distinguished clearly were not used for quantitative analysis. Approximately, two hundred cells per group were used to assess the influence of surface topography on cellular morphology.

**2.5. Human tenocyte viability, metabolic activity and proliferation**

Live/Dead® assay (BioSource International, Invitrogen, Ireland) was performed on days 1, 5 and 10 to assess cellular viability, as per manufacturer's protocol. Briefly, cells were washed 3 times with HBSS and exposed to the staining solution of calcein and ethidium homodimer. The cells were incubated at 37 °C for 45 min. Following staining, the cells were viewed using the BX51 Olympus fluorescence microscope and analysed using ImageJ.

Cell metabolic activity was determined using alamarBlue® assay on days 1, 5, and 10, as per manufacturer's protocol. Briefly, alamarBlue® dye was diluted with HBSS to make a 10 % (v/v) alamarBlue® solution. Media was removed from each well and 0.5 ml alamarBlue® solution was added to each well. Cell were incubated for 3 h at 37 °C; the absorbance of the alamarBlue® was measured at wavelengths of 550 nm and 595 nm using a micro plate reader (Varioskan Flash, Thermo Scientific, UK). The level of metabolic activity was calculated using the simplified method of calculating % reduction, according to the supplier's protocol.

Cell proliferation was assessed on days 1, 5, and 10, by counting DAPI stained cell nuclei, using the BX51 Olympus fluorescence microscope (please see section 2.3 for more details).

All experiments (viability, metabolic activity and proliferation) were repeated in three independent experiments and each experiment was performed in triplicate.

**2.6. Human tenocyte gene expression analysis**

A comprehensive gene expression analysis was conducted using TaqMan® Low Density Array (TLDA; Applied Biosystems, UK), grouping genes of interest as collagenous, non-collagenous, adhesion and housekeepers (**Table 1**).

Cell density of 25,000 cells per 1 $cm^2$ was seeded on the substrates and total RNA was extracted from human tenocytes on days 0, 1, 5 and 10. Total RNA was extracted using Trizol reagent method. Briefly, Trizol (400 $\mu$g/well, Sigma Aldrich, UK) was added to the cells for 15 min to disrupt the cellular membranes. Then, the Trizol solution was collected and chloroform (Sigma Aldrich, UK) was added to the solution and shaken vigorously for 15 sec. RT incubation for 5 min was followed. Then the upper aqueous phase containing the RNA was removed and mixed with isopropanol (Sigma Aldrich, UK) to obtain a pure RNA pellet. Subsequently, the RNA was used for the reverse-transcriptase reaction to synthesize the first strand of cDNA. cDNA (100 ng) and universal PCR mastermix (50 $\mu$l) were loaded into the fill reservoirs (100 $\mu$l / reservoir) and the plate was run according to manufacturer's instructions, using the Applied Biosystems 7900HT Real-Time PCR System and Applied Biosystems Sequence Detection Systems (SDS 2.3 and RQ manager 1.2) software. The thermal cycles were as follows: 50 °C for 2 min, 94.5 °C for 10 min, followed by 40 cycles of 97 °C for 30 sec and 59.7 °C for 1 min. Using the $2^{-\Delta Ct}$ method, mean Ct values of each target gene was normalised to the housekeeping gene values. To analyse the changes in gene expression between the isotropic control and the anisotropic substrates for each day, $2^{-\Delta\Delta Ct}$ method was used. The gene expression was then evaluated using hierarchical clustering software

(IPA software of complex 'omics data, Ingenuity® systems, Qiagen, USA) with the fold change compared to the time point control and a threshold set at 1.4.

### 2.7. *In vivo* study and analysis

The Animal Care Research Ethics Committee of NUI Galway approved all experimental protocols. For the tendon model, female Lewis rats (200g – 250g) were used, following a protocol described previously [50]. Briefly, surgery was performed under general anaesthesia. A small incision was made to the side of the knee, exposing the patellar tendon by moving the skin and opening the fascia. Using a punch biopsy, a 2mm in diameter circular defect was created at the centre of the tendon, allowing the creation of a consistent and reproducible injury, without compromising the mechanical integrity of the tendon. The tendon was wiped dry using sterile gauze. Circular sections of the structured substrates (2 mm in diameter) were secured at the injury site using a PLGA film, secured in place with sutures. The grooved substrates were aligned parallel to the gross tendon orientation (**Figure 1**). Following euthanisation, tissue samples were harvested at weeks 2, 4 and 12, fixed in 4% paraformaldehyde (Sigma Aldrich, Ireland), stored in sucrose (Sigma Aldrich, Ireland) and then fixed in freezing compound (Sigma Aldrich, Ireland). Twelve animals were used at each time point and structured substrates and autografts were randomly assigned to each contralateral patellar tendon. Cryo-sectioning was performed at Histotech (University of York, UK0. Sections (10 $\mu$m thick) were cut using a Leica CM 1950 cryostat (Leica Microsystems, Germany) on manual setting, operating at -20 °C and collected onto Superfrost® Plus glass slides (Thermo Scientific, UK). Sections were air dried at ambient temperature for 1 hour and stored desiccated at -80ºC until use. Tissue sections were then stained with haematoxylin-eosin (Sigma Aldrich, Ireland) and images were captured with an Olympus IX-81 inverted microscope (Olympus Corporation, Tokyo, Japan). Tissue sections were also stained with Picrosirius Red (Sigma Aldrich, Ireland) and images were captured with an Olympus polarised light microscope (Olympus Corporation, Tokyo, Japan). Picrosirius Red images were also used for quantitative tissue

morphometric analysis (ImageJ). For the subcutaneous study, female Lewis rats (200g – 250g) were used, following a protocol described previously [51]. Briefly, surgery was performed on rats under general anaesthesia. Incisions were made at the back of each animal, allowing insertion of a 0.5 cm x 0.5 cm structured substrate. The wound was then closed, using biodegradable sutures. Following euthanisation, the substrates were harvested at days 2 and 14 and were stained using DAPI and rhodamine conjugated phalloidin. Three animals were used per time point and at each animal all three structured substrates were implanted. Images were captured with an Olympus IX-81 inverted microscope (Olympus Corporation, Tokyo, Japan).

### 2.8. Statistical analysis

All data were analysed using GraphPad Prism® 5 (GraphPad Software, USA) and/or PASW Statistics 17.0 (SPSS Inc, IL). Analysis of variance (ANOVA) and Tukey's multiple comparison post-hoc tests were performed after confirming the following assumptions: (a) the distribution from which each of the samples was derived was normal; and (b) the variances of the population of the samples were equal to one another. Statistical significance was accepted at $p < 0.05$.

## 3. Results

### 3.1. Substrate analysis

Anisotropic PLGA substrates with constant groove and line width of 1,911.42 ± 37.50 nm and 2,101.78 ± 35.21 nm respectively and variable groove depth of 37.48 ± 3.4 nm, 317.29 ± 7.05 nm and 1,988.2 ± 195.3 nm were fabricated using standard photolithography followed by imprinting lithography. Isotropic / quasi-planar PLGA substrates were used as control, with an inherent Ra of 80.17 ± 28.92 nm over 10 $\mu m^2$ (**Figure 2**). Surface chemical analysis indicated that no significant differences in elemental composition were present amongst all experimental topographical groups (**Figure 3**). XPS spectra presented well-defined peaks corresponding to the presence of C, O and Si on all substrates. A reduction in O and an increase in C content were observed on control substrates relative to topographical substrates. Critically, octadecyltrichlorosilane contamination was not present, as assessed by the absence of a chlorine peak at 198-200 eV.

### 3.2. Human tenocyte morphometric analysis as a function of topography

Gross visual analysis of immunofluorescent images revealed that at all time points (1, 5 and 10 days), human tenocytes exhibited spread morphology on isotropic and imprinted substrates with groove depth of ~37 nm (**Figure 4A**). An aligned orientation and an elongated morphology, parallel to the substrate topography, was observed as early as 24 h in culture and was maintained for up to 10 days (longer culture time point assessed) on imprinted substrates with groove depth of ~317 nm and ~1,988 nm (**Figure 4A**).

Subsequently, a detailed quantitative analysis was carried out to assess the influence of the various topographies, including isotropic controls, on cellular morphometry. Tenocytes on isotropic controls and ~37 nm in depth substrates exhibited random alignment / orientation, with the major axis of the cells evenly distributed over 90 °. Whereas by increasing the groove depth to ~317 nm and ~1,988 nm, 80 % and 100 % respectively cellular alignment / elongation parallel to the substrate topography was observed (**Figure 4B**). Although cellular area (**Figure 4C**) and nuclei

aspect ratio (**Figure 4E**) were not significantly affected ($p > 0.05$) as a function of the substrate topography, cellular aspect ratio was significantly increased ($p < 0.005$; **Figure 4D**) as a function of increasing groove depth, resulting in increasingly fusiform tenocyte morphology. Indeed, tenocytes seeded on the isotropic and ~37 nm in depth substrates exhibited cellular aspect ratio of approximately 4, whereas by increasing the groove depth to ~317 nm and ~1,988 nm, the aspect ratio was increased to approximately 11 and 16 respectively.

### 3.3. Human tenocyte viability, metabolic activity and proliferation analysis as a function of topography

No significant differences ($p > 0.05$) in human tenocyte viability (**Figure S1A**), metabolic activity (**Figure S1B**) and proliferation (**Figure S1C**) were observed at any time point (1, 5 and 10 days), as a function of the different topographies relative to isotropic controls.

### 3.4. Human tenocyte gene analysis as a function of topography

Hierarchal clustering of the fold change (threshold of 1.4) in gene expression of human tenocytes on the anisotropic substrates, as compared to the isotropic control substrates, at the corresponding time points (day 1, 5 and 10) is presented in **Figure 5**. At day 1, an overall gene upregulation (e.g. collagenous, non-collagenous and adhesion) was observed only in tenocytes cultured on substrates with groove depth of 1,988 nm, whilst at day 10 tenocytes cultured on substrates with groove depth ~317 nm and ~1,988 nm were associated with more genes that were significantly upregulated than substrates with groove depth ~37 nm. At day 10, IBSP (bone sialoprotein) and ACAN (aggrecan) were significantly upregulated on all substrates.

### 3.5. Host tissue response as a function of topography

Haematoxylin-eosin staining at the tendon repair site showed a disorganised collagen fibre pattern for all anisotropic substrates (**Figure 6**), which was further verified with Picrosirius Red staining

(**Figure 7**). By week 12, collagen fibres from all treatments changed from green, indicative of collagen type III, to yellow / red, indicative of collagen type I (**Figure 7**). Complementary morphometric analysis of tendon fibre alignment demonstrated that only non-injured tendons had 100 % fibre distribution between -5 to 5 °, whilst the rest treatments exhibited less than 65% fibre distribution between -5 to 5 ° (**Figure 8**). In a subcutaneous model, when structured substrates were explanted and stained for DAPI and rhodamine conjugated phalloidin, no apparent cellular alignment was evidenced (**Figure S2**).

## 4. Discussion

Herein, we ventured to investigate the impact of groove depth (~37 nm, ~317 nm and ~1,988 nm), whilst maintain groove width (~1,911 nm) and line width (~2,102 nm) constant, on human tenocyte morphology and gene expression *in vitro* and on directional neotissue formation *in vivo*. The groove dimensions were selected on the basis that closely represent the topographical cues (dimensionality of collagen fibrils is in the region of 10 to 1,000 nm, whilst the dimensionality of collagen fibres is in the region of 1,000 to 20,000 nm [12]) that tenocytes are exposed to *in vivo*. The micro-scale groove depth was selected based on previous publications, where authors supported that pitch dimensionality smaller than 4000 nm induces efficient cellular contact guidance [40, 42, 52]. Furthermore, the cellular response to underlying topographies is enhanced when the feature pitch is similar to or smaller than the dimensions of the cell type being studied [53], facilitating contact with more than one discontinuity. This approach allows for directional alignment of the cells without physically restricting cells within individual groove features [54].

With respect to the morphometric analysis, it was observed that isotropic (control) substrates and substrates with a groove depth of ~37 nm, failed to induce any morphological changes in cultured tenocytes. Conversely, substrates with deeper grooves (~317 nm and ~1,988 nm) induced significant changes to the cytoskeleton morphology, but did not significantly influence nuclei morphology. Although, the mechano-transduction theory proposes that intracellular tension in elongated and aligned cytoskeleton actin filaments is transferred to the nucleus through cytoskeletal elements [55-60], this indifference in nuclei morphology may be attributed to the short time after culture on grooved substrates that nuclei aspect ratio was assessed.

No significant difference was observed in cell metabolic activity, viability and proliferation, between the experimental groups. This observation indicates that although both topography and mechanical stretching can induce similar bidirectional cell elongation, only mechanical loading, in excessive form, can activate apoptotic pathways [61-64].

Gene analysis clearly indicates that only substrates with groove depth of ~1,988 nm induced immediate (day 1) upregulation effects on cultured tenocytes, which was maintained for all culture time points. However, by day 10, bone sialoprotein, osteonectin, runt-related transcription factor 2, cartilage oligomeric protein and aggrecan were significantly upregulated on substrates with groove depth ~1,988 nm and bone sialoprotein and aggrecan were significantly upregulated on all substrates. These observations indicate possibly trans-differentiation of tenocytes towards osteogenic / chondrogenic lineage. Indeed, bone sialoprotein encodes non-collagenous components of bone ECM; runt-related transcription factor 2 promotes osteogenic differentiation; and osteonectin is a bone-specific protein that binds selectively to hydroxyapatite and collagen [65-68]. Similarly, cartilage oligomeric protein and aggrecan, although persistent in tendon, are primarily considered cartilage-specific molecules, mutations of which are associated with skeletal pathophysiologies [69-72]. We attribute this indicative trans-differentiation to the far from physiological substrate stiffness of the PLGA material employed in this study. Indeed, substrate stiffness has been shown to strongly regulate protein expression, cell phenotype maintenance and stem cell differentiation, with soft substrates observed to be neurogenically conductive and rigid substrates to be chondrogenic / osteogenic [73-76]. This implies that multifactorial, rather than mono-domain, approaches should be assessed in future studies, in accordance with previous observations, where it was suggested that topography should be combined with mechanical loading for physiological bovine tenocyte morphology maintenance [27].

Critically, herein, the *in vitro* work was followed up with two *in vivo* studies to elucidate the efficacy of nano and micro-scale topographical functionalisation in *de novo* tissue regeneration. None of the structured substrates induced neotissue formation parallel to the substrate topography in a tendon model. Further, in a subcutaneous model, none of the substrates induced cellular orientation parallel to the direction of the substrate topography. It is tempting to hypothesise that two-dimensional imprinted substrates are overwhelmed with body fluids and protein adsorption upon implantation, prohibiting favourable cell / material interaction at the substrate-tissue nano-bio-

interface and that three-dimensional fibrous constructs are more effective for directional neural [77-79], tendon [29, 35, 80], bone [81-83] and skin [84-86] neotissue formation and promote relatively enhanced cell growth, motility, matrix deposition and neotissue growth through the provision of a true three-dimensional environment.

## 5. Conclusions

Herein, we demonstrated that low nano topographical features (~37 nm groove depth) were not sufficient to induce physiological tenocyte morphology, as compared to ~317 nm and ~1,988 nm groove depth substrates. In two different animal models, the structured substrates failed to induce parallel to the underlined topography directional host cell growth and neotissue formation. Further, the rigid substrates used upregulated gene expression of bone and cartilage genes, suggesting tenocyte trans-differentiation towards osteogenic and chondrogenic lineages, respectively. Collectively, these data indicate that three-dimensional fibrous constructs are more promising for directional neotissue formation, whilst two-dimensional imprinted substrates can be used for optimal cell expansion *in vitro*, should multifactorial approaches that consider both surface topography and substrate stiffness be established.

## 6. Acknowledgements

This work was supported by: Enterprise Ireland, Collaborative Centre for Applied Nanotechnology (Project No: CCIRP-2007-CCAN-0509), under the Irish Government's National Development Plan 2007-2013 to DZ; Tyndall National Institute, SFI-funded National Access Programme (Project No: NAP382) to DZ; Health Research Board (Project No: HRA_POR/2011/84) to DZ; Irish Research Council, Government of Ireland Postgraduate Scholarship Scheme (Grant Agreement Number: GOIPG/2014/385) to KS and DZ. MB is a Science Foundation Ireland, Starting Investigator SIRG COFUND fellow (Project No: 11/SIRG/B2135). The authors would also like to acknowledge Ms B. Hasegawa for technical support.

## 7. Tables

**Table 1:** Genes and their transcripts, grouped as collagenous, non-collagenous, adhesion and housekeepers.

| Gene Name | Gene Symbol | NCBI Ref. Seq. | TaqMan® Transcript |
|---|---|---|---|
| **Collagenous** | | | |
| Collagen I | COL1A1 | NM_000088.3 | Hs00164004_m1 |
| Collagen III | COL3A1 | NM_000090.3 | Hs00943809_m1 |
| Collagen IV | COL4A1 | NM_001845.4 | Hs00266237_m1 |
| Collagen V | COL5A1 | NM_000093.3 | Hs00609088_m1 |
| Collagen VI | COL6A1 | NM_001848.2 | Hs00242448_m1 |
| Collagen XI | COL11A1 | NM_001854.3 | Hs01097664_m1 |
| Collagen XII | COL12A1 | NM_004370.5 | Hs00189184_m1 |
| Collagen XIV | COL14A1 | NM_021110.1 | Hs00966234_m1 |
| **Non-collagenous** | | | |
| Scleraxis Homolog A | SCXA | NM_001008271.1 | Hs03054634_g1 |
| Tenascin C | TNC | NM_002160.3 | Hs01115665_m1 |
| Biglycan | BGN | NM_001711.4 | Hs00156076_m1 |
| Decorin | DCN | NM_001920.3 | Hs00370384_m1 |
| Osteopontin | SPP1 | NM_00058.2 | Hs00959010_m1 |
| Alkaline Phosphatase | ALPL | NM_000478.4 | Hs01029144_m1 |
| Bone Sialoprotein | IBSP | NM_004967.3 | Hs00173720_m1 |
| Osteonectin | SPARC | NM_003118.2 | Hs00234160_m1 |
| Runt-related transcription factor 2 | RUNX2 | NM_001015051.3 | Hs00231692_m1 |
| Cartilage oligomeric | COMP | NM_001920.3 | Hs00164359_m1 |

| | | | |
|---|---|---|---|
| protein | | | |
| Matrix gla protein | MGP | NM_000900.3 | Hs00969490_m1 |
| Thrombospondin 4 | THBS4 | NM_003248.4 | Hs00170261_m1 |
| Fibromodulin | FMOD | NM_002203.3 | Hs00158127_m1 |
| Fibronectin | FN1 | NM_212482.1 | Hs00277509_m1 |
| Laminin | LAMA | NM_005559.3 | Hs00300550_m1 |
| Aggrecan | ACAN | NM_0011353.3 | Hs00153936_m1 |
| Versican | VCAN | NM_001126336.2 | Hs01007933_m1 |
| **Adhesion** | | | |
| Integrin α1 | ITGA1 | NM_181501.1 | Hs00235006_m1 |
| Integrin α2 | ITGA2 | NM_002203.3 | Hs00201927_m1 |
| Integrin α3 | ITGA3 | NM_002204.2 | Hs01076873_m1 |
| Integrin α4 | ITGA4 | NM_000885.4 | Hs00168433_m1 |
| Integrin α5 | ITGA5 | NM_002205.2 | Hs01547673_m1 |
| Integrin α6 | ITGA6 | NM_000210.2 | Hs01041011_m1 |
| Integrin α10 | ITGA10 | NM_003637.3 | Hs00174623_m1 |
| Integrin α11 | ITGA11 | NM_001004439.1 | Hs00201927_m1 |
| Integrin β1 | ITGB1 | NM_002211.3 | Hs00559595_m1 |
| Integrin β2 | ITGB2 | NM_000211.3 | Hs00164957_m1 |
| Integrin β3 | ITGB3 | NM_000212.2 | Hs01001469_m1 |
| Integrin β5 | ITGB5 | NM_002213.3 | Hs00174435_m1 |
| CD44 | CD44 | NM_000610.3 | Hs01075861_m1 |
| **Housekeeping** | | | |
| 18S ribosomal RNA | 18S rRNA | | Hs99999901_s1 |
| Topoisomerase (DNA) I | TOP1 | NM_003286.2 | Hs00243257_m1 |

| | | | |
|---|---|---|---|
| Eukaryotic translation initiation factor 4α | EIF4α | | Hs00756996_g1 |

**8. Figures**

**Figure 1:** For the tendon model, we induced an incision to the side of the leg (A) to expose the tendon by moving the skin (B). Using a 2 mm in diameter punch biopsy, we created a wound at the centre of the tendon, where the structured substrates were then inserted (C). The implants were secured using a PLGA film (D) and wounds were closed using biodegradable sutures (E).

**Figure 2:** AFM analysis of isotropic (A) and structured (B, C, D) substrates. Quantification of isotropic control roughness, groove width, line width and groove depth (E).

**Figure 3:** XPS analysis isotropic (Control) and structured substrates. Surface chemical analysis indicated no significant differences in elemental composition among all experimental topographical groups. Further, octadecyltrichlorosilane contamination was not detected, as evidenced by the absence of a chlorine peak at 198-200 eV.

**Figure 4:** DAPI (blue) and rhodamine conjugated phalloidin (red) indicates that tenocytes aligned parallel to the substrate topography of groove depths of ~317 nm and ~1,988 nm, whilst a random morphology was observed on isotropic substrates and substrates with groove depth of ~37 nm (A). This was further confirmed, when the angle of cells parallel to the underlying topography was between 0 – 20 ° on substrates with groove depth of ~317 nm and ~1,988 nm (B). Substrates with groove depth of ~317 nm and ~1,988 nm induced the highest ($p < 0.005$) cytoskeleton elongation (D). No significant difference ($p > 0.05$) was observed in cellular area (C) and nuclei aspect ratio (E) as a function of surface topography. Note: Approximately 200 cells were used to assess the influence of surface topography on cellular morphology.

**Figure 5:** Gene analysis demonstrates an overall gene upregulation at day 1 only on cells seeded on ~1,988 nm in depth substrates, whilst at day 10 substrates with groove depth ~317 nm and ~1,988

nm had more upregulated genes than substrates with groove depth of ~37 nm. At day 10, bone sialoprotein and aggrecan were upregulated on all substrates.

**Figure 6:** Histological examination at the tendon repair site using haematoxylin-eosin staining showed a disorganised collagen fibre pattern for all implanted anisotropic substrates. Nuclei are stained blue, whereas cytoskeleton and extracellular matrix demonstrate varying degrees of pink staining.

**Figure 7:** Histological analysis using Picrosirius Red staining and subsequent polarised light analysis demonstrated that by week 12 all treatments gave rise to collagen type I (yellow / red). At early time points (2 and 4 weeks) collagen type III (green) was evidenced.

**Figure 8:** Collagen fibre morphometric analysis indicated that only non-injured tendons had 100% fibre distribution between -5 to 5 °, whilst the rest treatments exhibited less than 65% fibre distribution between -5 to 5 °.

**9. References**

[1] Liu C, Aschbacher-Smith L, Barthelery N, Dyment N, Butler D, Wylie C. What we should know before using tissue engineering techniques to repair injured tendons: A developmental biology perspective. Tissue Eng B 2011;17:165-176.

[2] Zhang X, Bogdanowicz D, Erisken C, Lee N, Lu H. Biomimetic scaffold design for functional and integrative tendon repair. J Should Elb Surg 2012;21:266-277.

[3] Longo U, Lamberti A, Petrillo S, Maffulli N, Denaro V. Scaffolds in tendon tissue engineering. Stem Cells Intern 2012;2012:517165.

[4] Liu Y, Ramanath H, Wang D. Tendon tissue engineering using scaffold enhancing strategies. Trends Biotechnol 2008;26:201-209.

[5] Cigognini D, Lomas A, Kumar P, Satyam A, English A, Azeem A, Pandit A, Zeugolis D. Engineering in vitro microenvironments for cell based therapies and drug discovery. Drug Discov Tod 2013;18:1099-1108.

[6] Bagnaninchi P, Yang Y, Haj A, Maffulli N. Tissue engineeering for tendon repair. Br J Sports Med 2007;41:1-5.

[7] James R, Kesturu G, Balian G, Chhabra A. Tendon: Biology, biomechanics, repair, growth factors, and evolving treatment options. J Hand Surg 2008;33:102-112.

[8] Butler D, Juncosa-Melvin N, Boivin G, Galloway M, Shearn J, Gooch C, Awad H. Functional tissue engineering for tendon repair: A multidisciplinary strategy using mesenchymal stem cells, bioscaffolds, and mechanical stimulation. J Orthop Res 2008;26:1-9.

[9] Gaspar D, Spanoudes K, Holladay C, Pandit A, Zeugolis D. Progress in cell-based therapies for tendon repair. Adv Drug Deliv Rev 2015;84:240-256.

[10] Lomas A, Ryan C, Sorushanova A, Shologu N, Sideri A, Tsioli V, Fthenakis G, Tzora A, Skoufos I, Quinlan L, O'Laighin G, Mullen A, Kelly J, Kearns S, Biggs M, Pandit A, Zeugolis D. The past, present and future in scaffold-based tendon treatments. Adv Drug Deliv Rev In Press.

[11] Abbah S, Spanoudes K, O'Brien T, Pandit A, Zeugolis D. Assessment of stem cell carriers for tendon tissue engineering in pre-clinical models. Stem Cell Res Ther 2014;5:38.

[12] Spanoudes K, Gaspar D, Pandit A, Zeugolis D. The biophysical, biochemical, and biological toolbox for tenogenic phenotype maintenance in vitro. Trends Biotechnol 2014;32:474-482.

[13] Docheva D, Müller S, Majewski M, Evans C. Biologics for tendon repair. Adv Drug Deliv Rev In Press.

[14] Kong Y, Tu C, Donovan P, Yee A. Expression of Oct4 in human embryonic stem cells is dependent on nanotopographical configuration. Acta Biomater 2013;9:6369-6380.

[15] Yang K, Jung K, Ko E, Kim J, Park K, Kim J, Cho S. Nanotopographical manipulation of focal adhesion formation for enhanced differentiation of human neural stem cells. ACS Appl Mater Interf 2013;5:10529-10540.

[16] Yang K, Jung H, Lee H, Lee J, Kim S, Song K, Cheong E, Bang J, Im S, Cho S. Multiscale, hierarchically patterned topography for directing human neural stem cells into functional neurons. ACS Nano 2014;8:7809-7822.

[17] Yang K, Park E, Lee J, Kim I, Hong K, Park K, Cho S, Yang H. Biodegradable nanotopography combined with neurotrophic signals enhances contact guidance and neuronal differentiation of human neural stem cells. Macromol Biosci In Press.

[18] Yang H, Lee B, Tsui J, Macadangdang J, Jang S, Im S, Kim D. Electroconductive nanopatterned substrates for enhanced myogenic differentiation and maturation. Adv Healthc Mater In Press.

[19] Lee E, Im S, Hwang N. Efficient myogenic commitment of human mesenchymal stem cells on biomimetic materials replicating myoblast topography. Biotechnol J 2014;9:1604-1612.

[20] Ahn E, Kim Y, Kshitiz G, An S, Afzal J, Lee S, Kwak M, Suh K, Kim D, Levchenko A. Spatial control of adult stem cell fate using nanotopographic cues. Biomater 2014;35:2401-2410.

[21] Harris G, Piroli M, Jabbarzadeh E. Deconstructing the effects of matrix elasticity and geometry in mesenchymal stem cell lineage commitment. Adv Funct Mater 2014;24:2396-2403.

[22] Kim J, Bae W, Choung H, Lim K, Seonwoo H, Jeong H, Suh K, Jeon N, Choung P, Chung J. Multiscale patterned transplantable stem cell patches for bone tissue regeneration. Biomater 2014;35:9058-9067.

[23] Nemeth C, Janebodin K, Yuan A, Dennis J, Reyes M, Kim D. Enhanced chondrogenic differentiation of dental pulp stem cells using nanopatterned PEG-GelMA-HA hydrogels. Tissue Eng A 2014;20:2817-2829.

[24] Sjöström T, McNamara L, Meek R, Dalby M, Su B. 2D and 3D nanopatterning of titanium for enhancing osteoinduction of stem cells at implant surfaces. Adv Healthc Mater 2013;2:1285-1293.

[25] de Peppo G, Agheli H, Karlsson C, Ekström K, Brisby H, Lennerås M, Gustafsson S, Sjövall P, Johansson A, Olsson E, Lausmaa J, Thomsen P, Petronis S. Osteogenic response of human mesenchymal stem cells to well-defined nanoscale topography in vitro. Int J Nanomedicine 2014;9:2499-2515.

[26] Ladd M, Lee S, Stitzel J, Atala A, Yoo J. Co-electrospun dual scaffolding system with potential for muscle-tendon junction tissue engineering. Biomater 2011;32:1549-1559.

[27] English A, Azeem A, Gaspar D, Keane K, Kumar P, Keeney M, Rooney N, Pandit A, Zeugolis D. Preferential cell response to anisotropic electro-spun fibrous scaffolds under tension-free conditions. J Mater Sci Mater Med 2012;23:137-148.

[28] Chen B, Wang B, Zhang W, Zhou G, Cao Y, Liu W. In vivo tendon engineering with skeletal muscle derived cells in a mouse model. Biomater 2012;33:6086-6097.

[29] Liu W, Chen B, Deng D, Xu F, Cui L, Cao Y. Repair of tendon defect with dermal fibroblast engineered tendon in a porcine model. Tissue Eng 2006;12:775-788.

[30] Sahoo S, Toh S, Goh J. A bFGF-releasing silk/PLGA-based biohybrid scaffold for ligament/tendon tissue engineering using mesenchymal progenitor cells. Biomater 2010;31:2990-2998.

[31] Yin Z, Chen X, Chen J, Shen W, Hieu-Nguyen T, Gao L, Ouyang H. The regulation of tendon stem cell differentiation by the alignment of nanofibers. Biomater 2010;31:2163-2175.

[32] Zeugolis D, Paul G, Attenburrow G. Cross-linking of extruded collagen fibres - A biomimetic three-dimensional scaffold for tissue engineering applications. J Biomed Mater Res A 2009;89:895-908.

[33] Kato Y, Dunn M, Zawadsky J, Tria A, Silver F. Regeneration of Achilles tendon with a collagen tendon prosthesis. Results of a one-year implantation study. J Bone Joint Surg 1991;73:561-574.

[34] Cavallaro J, Kemp P, Kraus K. Collagen fabrics as biomaterials. Biotechn Bioeng 1994;43:781-791.

[35] Enea D, Gwynne J, Kew S, Arumugam M, Shepherd J, Brooks R, Ghose S, Best S, Cameron R, Rushton N. Collagen fibre implant for tendon and ligament biological augmentation. in vivo study in an ovine model. Knee Surg Sports Traumatol Arthrosc 2013;21:1783-1793.

[36] Kishore V, Bullock W, Sun X, VanDyke W, Akkus O. Tenogenic differentiation of human MSCs induced by the topography of electrochemically aligned collagen threads. Biomater 2012;33:2137-2144.

[37] Cheng X, Gurkan U, Dehen C, Tate M, Hillhouse H, Simpson G, Akkus O. An electrochemical fabrication process for the assembly of anisotropically oriented collagen bundles. Biomater 2008;29:3278-3288.

[38] Zhu J, Li J, Wang B, Zhang W, Zhou G, Cao Y, Liu W. The regulation of phenotype of cultured tenocytes by microgrooved surface structure. Biomater 2010;31:6952-6958.

[39] Kapoor A, Caporali E, Kenis P, Stewart M. Microtopographically patterned surfaces promote the alignment of tenocytes and extracellular collagen. Acta Biomater 2010;6:2580-2589.

[40] Tong W, Shen W, Yeung C, Zhao Y, Cheng S, Chu P, Chan D, Chan G, Cheung K, Yeung K, Lam Y. Functional replication of the tendon tissue microenvironment by a bioimprinted substrate and the support of tenocytic differentiation of mesenchymal stem cells. Biomater 2012;33:7686-7698.

[41] Dalby M, Riehle M, Yarwood S, Wilkinson C, Curtis A. Nucleus alignment and cell signaling in fibroblasts: response to a micro-grooved topography. Experim Cell Res 2003;284:272-280.

[42] Biggs M, Richards R, McFarlane S, Wilkinson C, Oreffo R, Dalby M. Adhesion formation of primary human osteoblasts and the functional response of mesenchymal stem cells to 330nm deep microgrooves. J Royal Soc Interf 2008;5:1231-1242.

[43] Chen W, Villa-Diaz L, Sun Y, Weng S, Kim J, Lam R, Han L, Fan R, Krebsbach P, Fu J. Nanotopography influences adhesion, spreading, and self-renewal of human embryonic stem cells. ACS Nano 2012;6:4094-4103.

[44] Unadkat H, Hulsman M, Cornelissen K, Papenburg B, Truckenmuller R, Post G, Uetz M, Reinders M, Stamatialis D, van Blitterswijk C, de Boer J. An algorithm-based topographical biomaterials library to instruct cell fate. Proc Natl Acad Sci USA 2011;108:16565-16570.

[45] Chen S, Jones J, Xu Y, Low H, Anderson J, Leong K. Characterization of topographical effects on macrophage behavior in a foreign body response model. Biomater 2010;31:3479-3491.

[46] Fisher O, Khademhosseini A, Langer R, Peppas N. Bioinspired materials for controlling stem cell fate. Acc Chem Res 2009;43:419-428.

[47] Brunetti V, Maiorano G, Rizzello L, Sorce B, Sabella S, Cingolani R, Pompa P. Neurons sense nanoscale roughness with nanometer sensitivity. Proc Natl Acad Sci USA 2010;107:6264-6269.

[48] Bauer A, Jackson T, Jiang Y. Topography of extracellular matrix mediates vascular morphogenesis and migration speeds in angiogenesis. PLoS Comput Biol 2009;5:e1000445.

[49] Azeem A, English A, Kumar P, Satyam A, Biggs M, Jones E, Tripathi B, Basu N, Henkel J, Vaquette C, Rooney N, Riley G, O'Riordan A, Cross G, Ivanovski S, Hutmacher D, Pandit A, Zeugolis D. The influence of anisotropic nano- to micro- topography on in vitro and in vivo osteogenesis. Nanomedicine 2015;10:693-711.

[50] Zhang J, Li B, Wang J. The role of engineered tendon matrix in the stemness of tendon stem cells in vitro and the promotion of tendon-like tissue formation in vivo. Biomater 2011;32:6972-6981.

[51] Keeney M, van den Beucken J, van der Kraan P, Jansen J, Pandit A. The ability of a collagen/calcium phosphate scaffold to act as its own vector for gene delivery and to promote bone formation via transfection with VEGF(165). Biomater 2010;31:2893-2902.

[52] Cassidy J, Roberts J, Smith C, Robertson M, White K, Biggs M, Oreffo R, Dalby M. Osteogenic lineage restriction by osteoprogenitors cultured on nanometric grooved surfaces: The role of focal adhesion maturation. Acta Biomater 2014;10:651-660.

[53] Clark P, Connolly P, Curtis A, Dow J, Wilkinson C. Topographical control of cell behaviour. I. Simple step cues. Development 1987;99:439-448.

[54] Clark P, Connolly P, Moores G. Cell guidance by micropatterned adhesiveness in vitro. J Cell Sc 1992;103:287-292.

[55] Ingber D. Tensegrity: The architectural basis of cellular mechanotransduction. Annu Rev Physiol 1997;59:575-599.

[56] Pierres A, Benoliel A, Bongrand P. Cell fitting to adhesive surfaces: A prerequisite to firm attachment and subsequent events. Eur Cell Mater 2002;3:31-45.

[57] Pavalko F, Norvell S, Burr D, Turner C, Duncan R, Bidwell J. A model for mechanotransduction in bone cells: The load-bearing mechanosomes. J Cell Biochem 2003;88:104-112.

[58] Orr A, Helmke B, Blackman B, Schwartz M. Mechanisms of mechanotransduction. Dev Cell 2006;10:11-20.

[59] Dalby M, Biggs M, Gadegaard N, Kalna G, Wilkinson C, Curtis A. Nanotopographical stimulation of mechanotransduction and changes in interphase centromere positioning. J Cell Biochem 2007;100:326-338.

[60] Ingber D. From cellular mechanotransduction to biologically inspired engineering: 2009 Pritzker Award Lecture, BMES Annual Meeting October 10, 2009. Ann Biomed Eng 2010;38:1148-1161.

[61] Noble B, Peet N, Stevens H, Brabbs A, Mosley J, Reilly G, Reeve J, Skerry T, Lanyon L. Mechanical loading: Biphasic osteocyte survival and targeting of osteoclasts for bone destruction in rat cortical bone. Am J Physiol Cell Physiol 2003;284:C934–C943.

[62] Scott A, Khan K, Heer J, Cook J, Lian O, Duronio V. High strain mechanical loading rapidly induces tendon apoptosis: An ex vivo rat tibialis anterior model. Br J Sports Med 2005;39:1-4.

[63] Egerbacher M, Arnoczky S, Caballero O, Lavagnino M, Gardner K. Loss of homeostatic tension induces apoptosis in tendon cells: An in vitro study. Clin Orthop Relat Res 2008;466:1562-1568.

[64] Kuo Y, Wu L, Sun J, Chen M, Sun M, Tsuang Y. Mechanical stress-induced apoptosis of nucleus pulposus cells: An in vitro and in vivo rat model. J Orthop Sci 2014;19:313-322.

[65] Fowlkes J, Bunn R, Liu L, Wahl E, Coleman H, Cockrell G, Perrien D, Lumpkin C, Thrailkill K. Runt-related transcription factor 2 (RUNX2) and RUNX2-related osteogenic genes are down-regulated throughout osteogenesis in type 1 diabetes mellitus. Endocrinology 2008;149:1697-1704.

[66] Wu C, Miron R, Sculean A, Kaskel S, Doert T, Schulze R, Zhang Y. Proliferation, differentiation and gene expression of osteoblasts in boron-containing associated with dexamethasone deliver from mesoporous bioactive glass scaffolds. Biomater 2011;32:7068-7078.

[67] Khan M, Donos N, Salih V, Brett P. The enhanced modulation of key bone matrix components by modified titanium implant surfaces. Bone 2012;50:1-8.

[68] Termine J, Kleinman H, Whitson S, Conn K, McGarvey M, Martin G. Osteonectin, a bone-specific protein linking mineral to collagen. Cell 1981;26:95-105.

[69] Posey K, Hecht J. The role of cartilage oligomeric matrix protein (COMP) in skeletal disease. Curr Drug Targets 2008;9:869-877.

[70] Geng H, Carlsen S, Nandakumar K, Holmdahl R, Aspberg A, Oldberg A, Mattsson R. Cartilage oligomeric matrix protein deficiency promotes early onset and the chronic development of collagen-induced arthritis. Arthr Res & Ther 2008;10:R134.

[71] Kiani C, Chen L, Wu Y, Yee A, Yang B. Structure and function of aggrecan. Cell Res 2002;12:19-32.

[72] Hardingham T, Fosang A, Dudhia J. The structure, function and turnover of aggrecan, the large aggregating proteoglycan from cartilage. Eur J Clin Chem Clin Biochem 1994;32:249-257.

[73] Engler A, Sen S, Sweeney H, Discher D. Matrix elasticity directs stem cell lineage specification. Cell 2006;126:677-689.

[74] Evans N, Minelli C, Gentleman E, LaPointe V, Patankar S, Kallivretaki M, Chen X, Roberts C, Stevens M. Substrate stiffness affects early differentiation events in embryonic stem cells. Eur Cell Mater 2009;18:1-14.

[75] Keogh M, O'Brien F, Daly J. Substrate stiffness and contractile behaviour modulate the functional maturation of osteoblasts on a collagen–GAG scaffold. Acta Biomater 2010;6:4305-4313.

[76] Mullen C, Haugh M, Schaffler M, Majeska R, McNamara L. Osteocyte differentiation is regulated by extracellular matrix stiffness and intercellular separation. J Mech Behav Biomed Mater 2013;28:183-194.

[77] Gelain F, Panseri S, Antonini S, Cunha C, Donega M, Lowery J, Taraballi F, Cerri G, Montagna M, Baldissera F, Vescovi A. Transplantation of nanostructured composite scaffolds results in the regeneration of chronically injured spinal cords. ACS Nano 2011;5:227-236.

[78] Weightman A, Jenkins S, Pickard M, Chari D, Yang Y. Alignment of multiple glial cell populations in 3D nanofiber scaffolds: Toward the development of multicellular implantable scaffolds for repair of neural injury. Nanomedicine 2014;10:291-295.

[79] Binan L, Tendey C, De Crescenzo G, El Ayoubi R, Ajji A, Jolicoeur M. Differentiation of neuronal stem cells into motor neurons using electrospun poly-L-lactic acid/gelatin scaffold. Biomater 2014;35:664-674.

[80] Xu L, Cao D, Liu W, Zhou G, Zhang W, Cao Y. In vivo engineering of a functional tendon sheath in a hen model. Biomater 2010;31:3894-3902.

[81] Ngiam M, Liao S, Patil A, Cheng Z, Chan C, Ramakrishna S. The fabrication of nano-hydroxyapatite on PLGA and PLGA/collagen nanofibrous composite scaffolds and their effects in osteoblastic behavior for bone tissue engineering. Bone 2009;45:4-16.

[82] Prabhakaran M, Venugopal J, Ramakrishna S. Electrospun nanostructured scaffolds for bone tissue engineering. Acta Biomater 2009;5:2884-2893.

[83] Cipitria A, Lange C, Schell H, Wagermaier W, Reichert J, Hutmacher D, Fratzl P, Duda G. Porous scaffold architecture guides tissue formation. J Bone Miner Res 2012;27:1275-1288.

[84] Chen H, Huang J, Yu J, Liu S, Gu P. Electrospun chitosan-graft-poly (ε -caprolactone)/poly (ε-caprolactone) cationic nanofibrous mats as potential scaffolds for skin tissue engineering. Int J Biol Macromol 2011;48:13-19.

[85] Yang Y, Xia T, Chen F, Wei W, Liu C, He S, Li X. Electrospun fibers with plasmid bFGF polyplex loadings promote skin wound healing in diabetic rats. Mol Pharm 2011;9:48-58.

[86] Vatankhah E, Prabhakaran M, Jin G, Ghasemi-Mobarakeh L, Ramakrishna S. Development of nanofibrous cellulose acetate/gelatin skin substitutes for variety wound treatment applications. J Biomater Appl 2014;28:909-921.

**Figure 1**

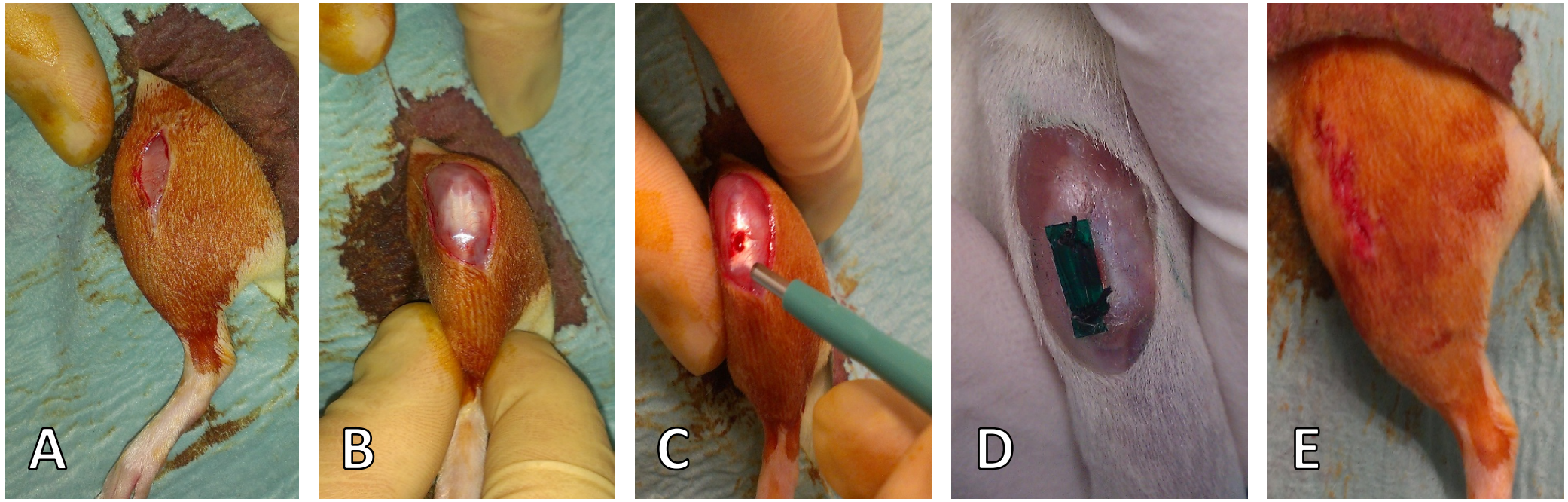

Figure 2

A

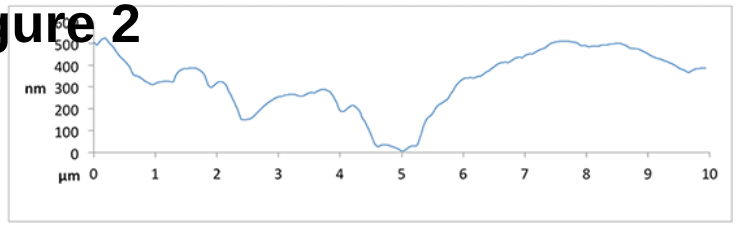


B

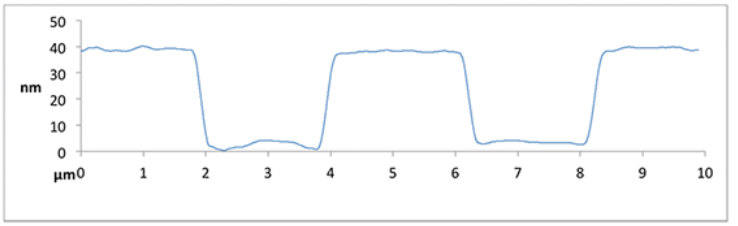


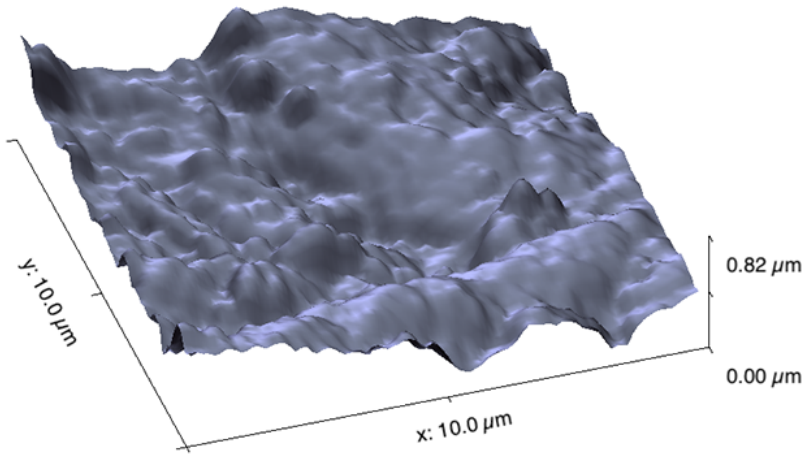


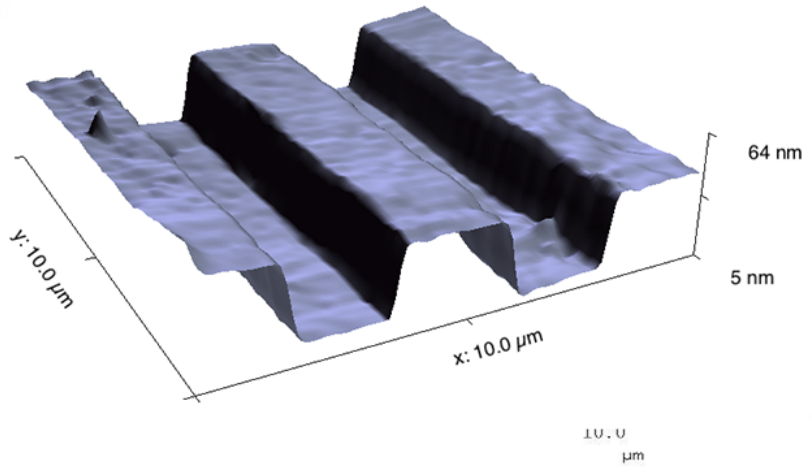


C

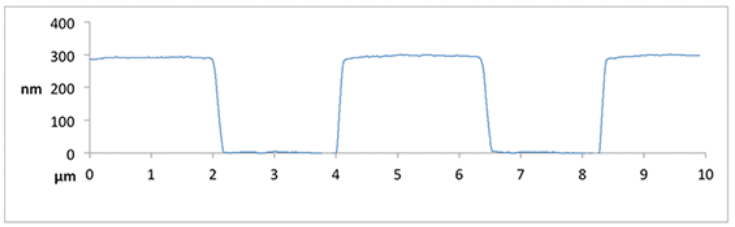


D

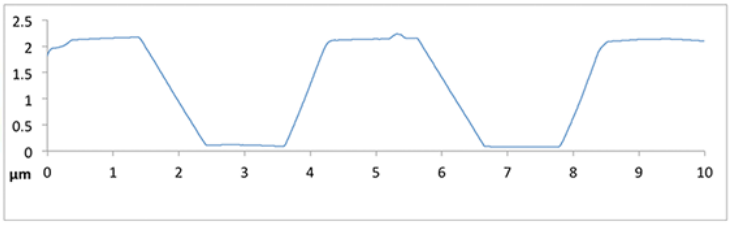


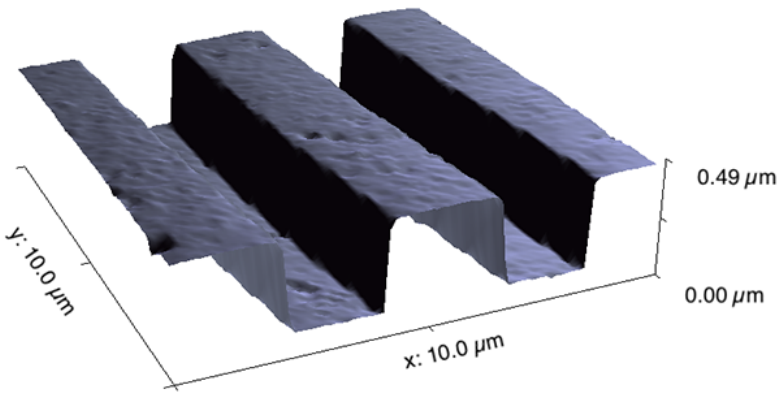


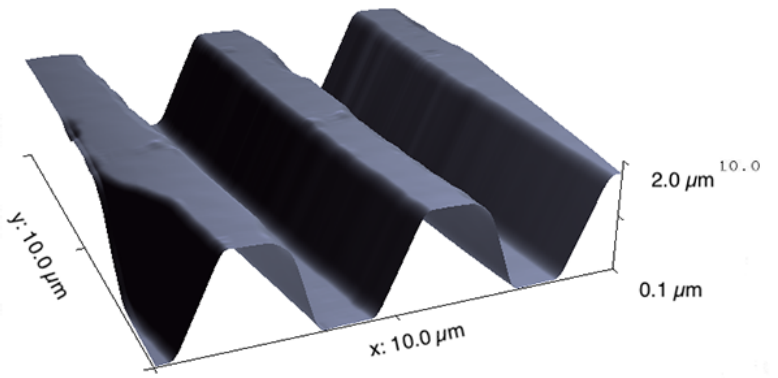


E

| AFM analysis of imprinted PLGA substrates | | | |
|---|---|---|---|
| Roughness ($R_a$) of isotropic control over 10 μm$^2$ (A) 80.168 ± 28.92 nm | | | |
| Groove Width (nm) | 1911.42 ± 37.50 | Line Width (nm) | 2101.78 ± 35.21 |
| Groove Depth (nm) | (B) 37.48 ± 3.4 | (C) 317.29 ± 7.05 | (D) 1988.2 ±195.3 |

Figure 3

## Elemental Composition (%)

| | O 1s | C 1s | Si 2p |
|---|---|---|---|
| **Control** | 23.9 | 70.1 | 6.0 |
| **37 nm** | 35.9 | 61.0 | 3.1 |
| **317 nm** | 37.7 | 57.0 | 5.3 |
| **1988 nm** | 33.0 | 63.6 | 3.3 |

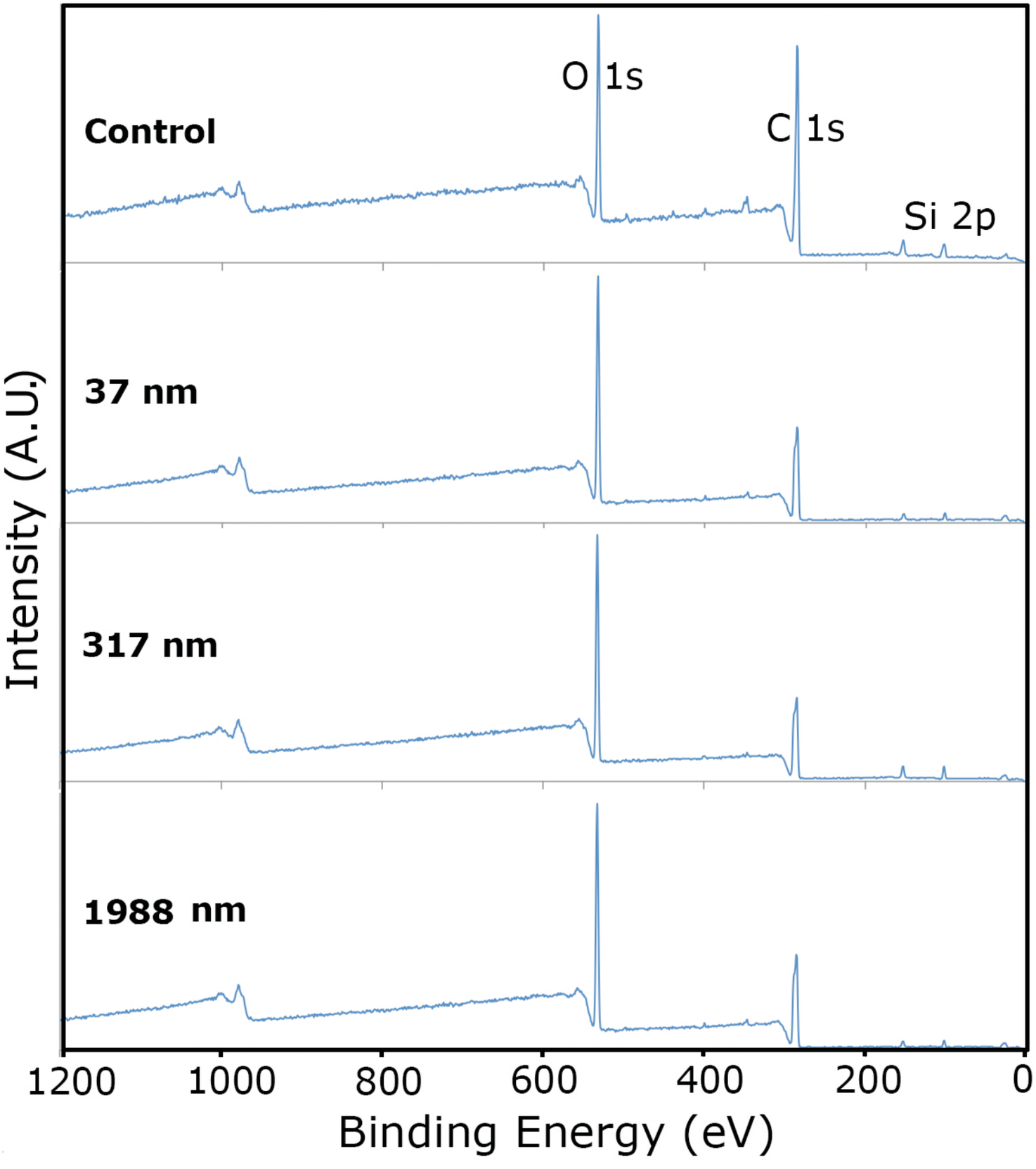

Figure 4

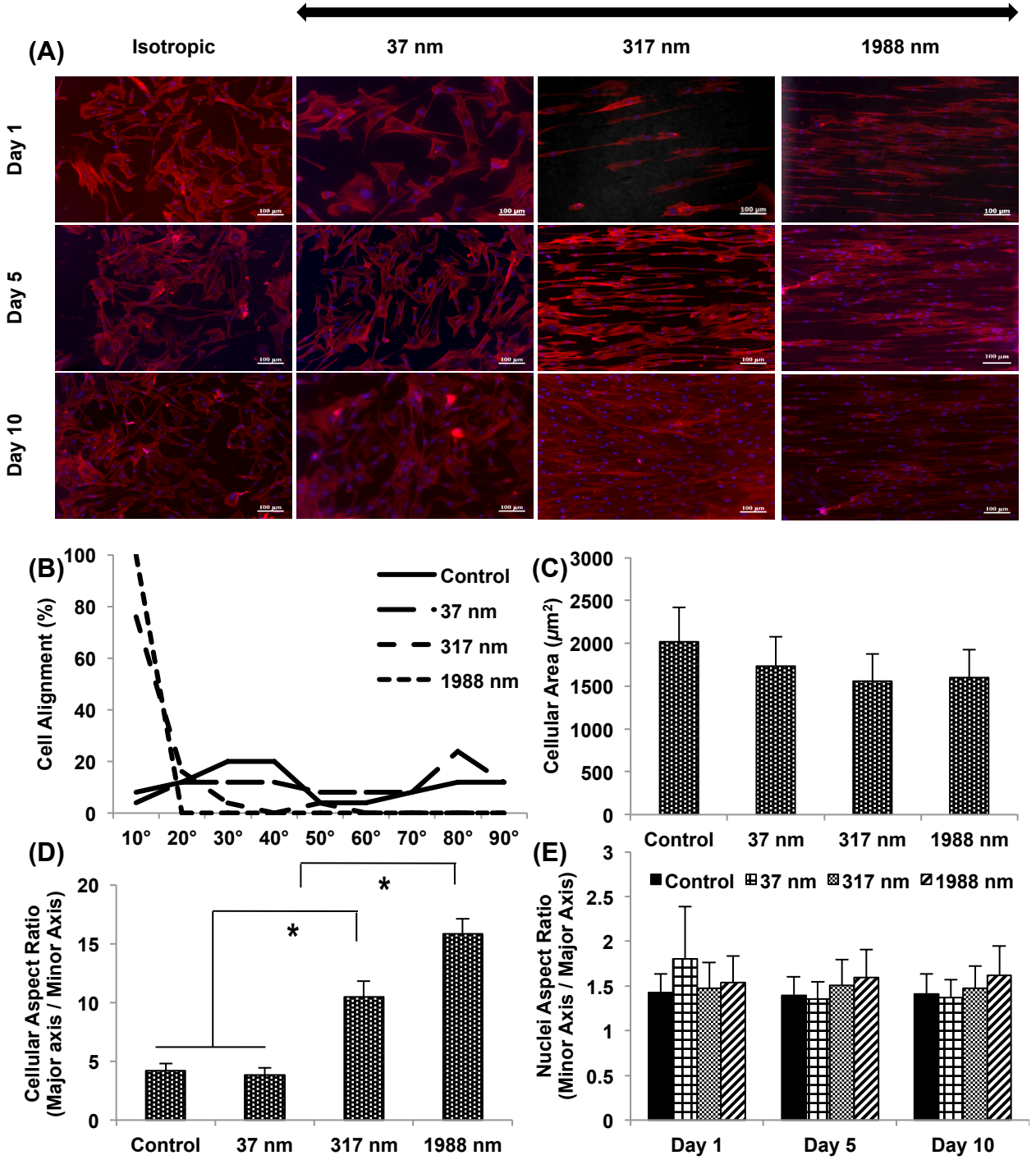
(A)
Isotropic
37 nm
317 nm
1988 nm
Day 1
Day 5
Day 10
(B)
Cell Alignment (%)
Control
37 nm
317 nm
1988 nm
10° 20° 30° 40° 50° 60° 70° 80° 90°
(C)
Cellular Area (μm²)
Control
37 nm
317 nm
1988 nm
(D)
Cellular Aspect Ratio (Major axis / Minor Axis)
Control
37 nm
317 nm
1988 nm
(E)
Nuclei Aspect Ratio (Minor Axis / Major Axis)
Control
37 nm
317 nm
1988 nm
Day 1
Day 5
Day 10

Figure 5

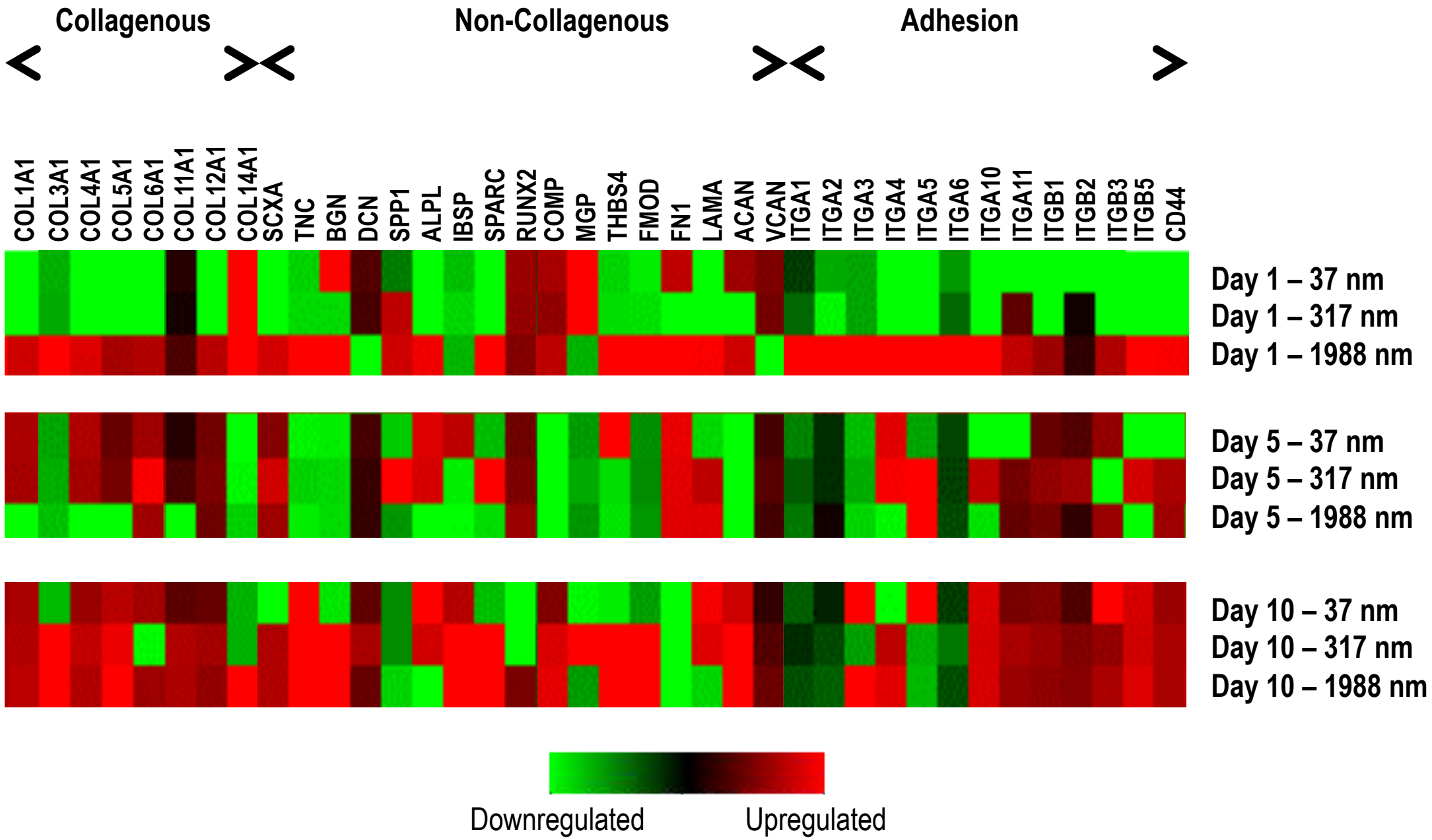
Collagenous
Non-Collagenous
Adhesion
COL1A1
COL3A1
COL4A1
COL5A1
COL6A1
COL11A1
COL12A1
COL14A1
SCXA
TNC
BGN
DCN
SPP1
ALPL
IBSP
SPARC
RUNX2
COMP
MGP
THBS4
FMOD
FN1
LAMA
ACAN
VCAN
ITGA1
ITGA2
ITGA3
ITGA4
ITGA5
ITGA6
ITGA10
ITGA11
ITGB1
ITGB2
ITGB3
ITGB5
CD44
Day 1 – 37 nm
Day 1 – 317 nm
Day 1 – 1988 nm
Day 5 – 37 nm
Day 5 – 317 nm
Day 5 – 1988 nm
Day 10 – 37 nm
Day 10 – 317 nm
Day 10 – 1988 nm
Downregulated
Upregulated

Figure 6

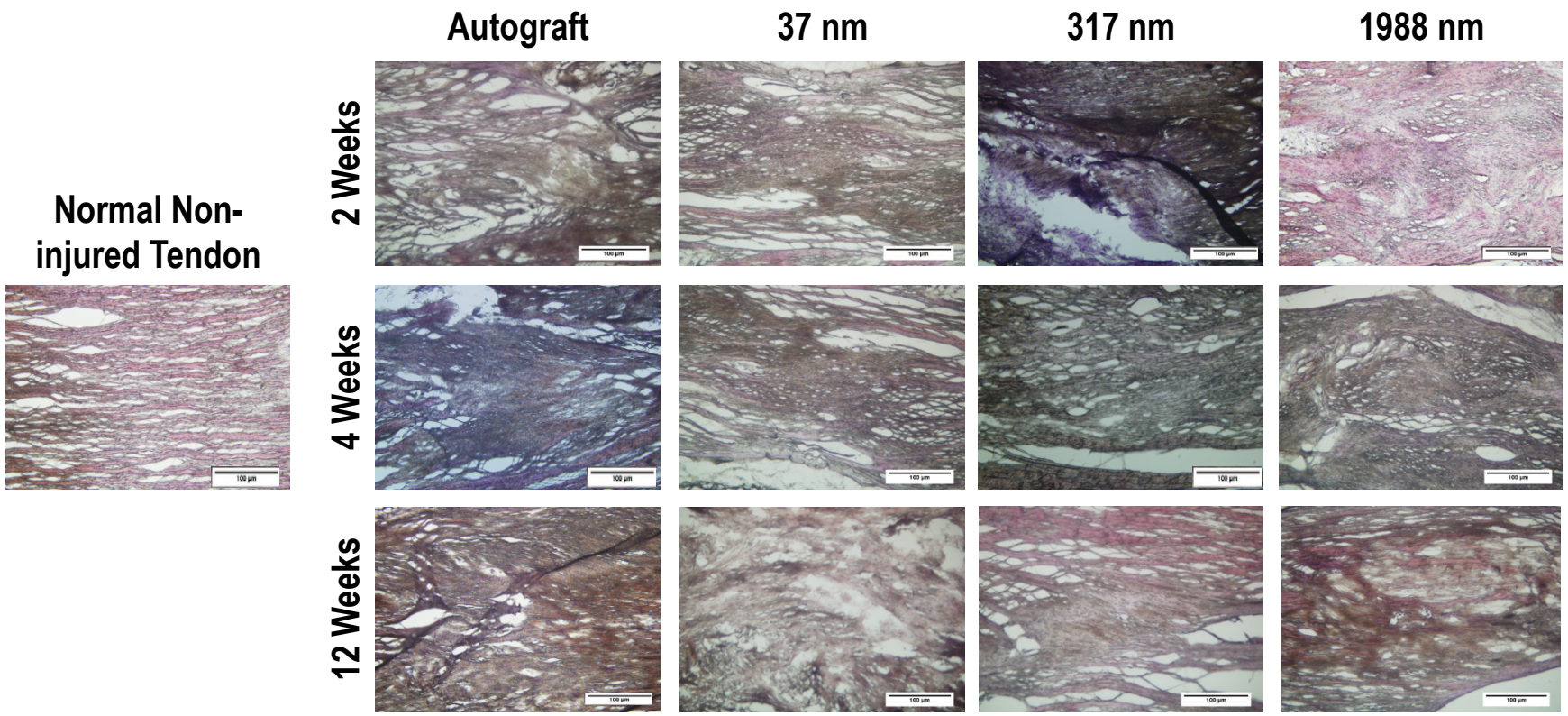
Autograft
37 nm
317 nm
1988 nm
2 Weeks
4 Weeks
12 Weeks
Normal Non-injured Tendon

Figure 7

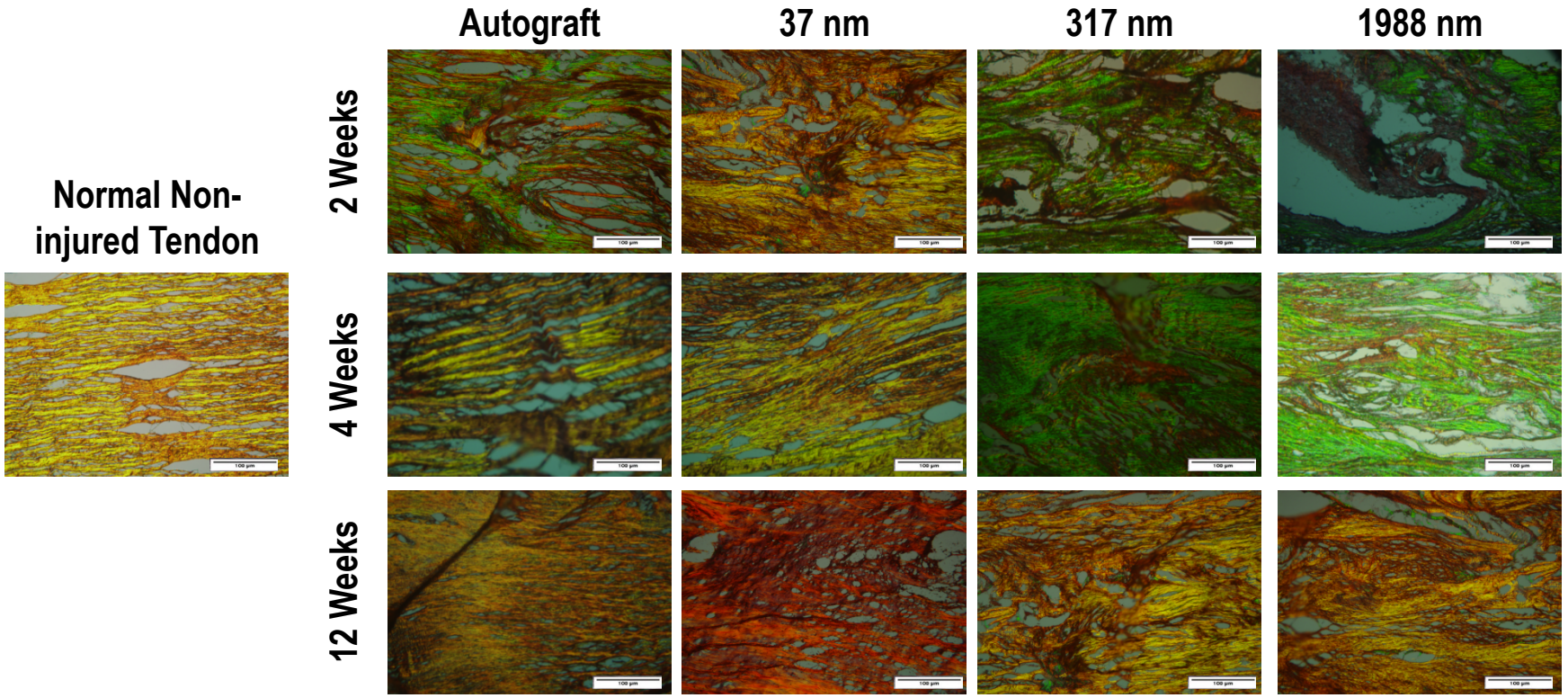
Autograft
37 nm
317 nm
1988 nm
Normal Non-injured Tendon
2 Weeks
4 Weeks
12 Weeks

Figure 8

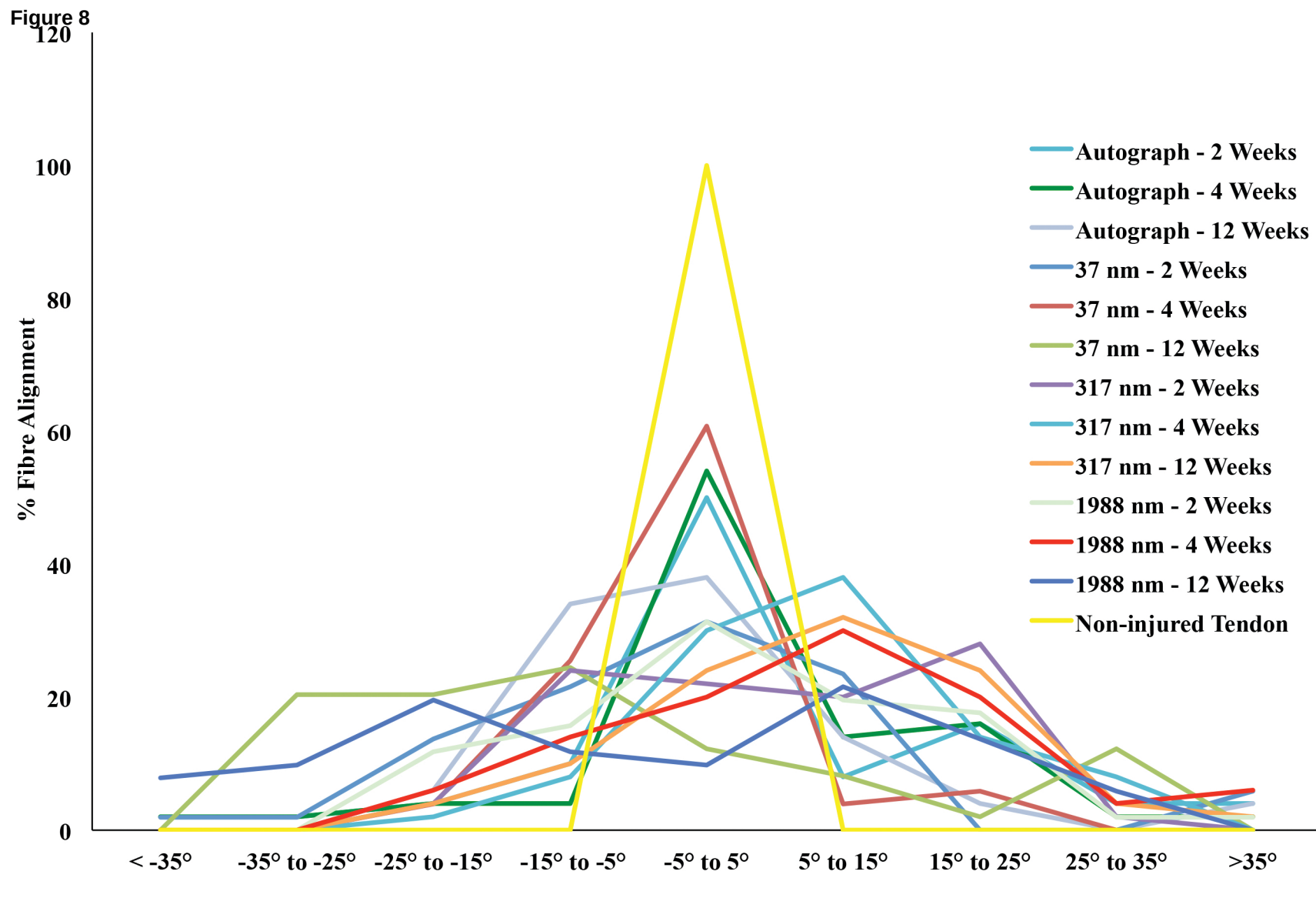
120
100
80
60
40
20
0
% Fibre Alignment
< -35°
-35° to -25°
-25° to -15°
-15° to -5°
-5° to 5°
5° to 15°
15° to 25°
25° to 35°
>35°
Autograph - 2 Weeks
Autograph - 4 Weeks
Autograph - 12 Weeks
37 nm - 2 Weeks
37 nm - 4 Weeks
37 nm - 12 Weeks
317 nm - 2 Weeks
317 nm - 4 Weeks
317 nm - 12 Weeks
1988 nm - 2 Weeks
1988 nm - 4 Weeks
1988 nm - 12 Weeks
Non-injured Tendon

| | Groove Width: 1911 nm<br>Line Width: 2102 nm<br>Groove Depth: 37 nm | Groove Width: 1911 nm<br>Line Width: 2102 nm<br>Groove Depth: 317 nm | Groove Width: 1911 nm<br>Line Width: 2102 nm<br>Groove Depth: 1988 nm |
|---|---|---|---|
| Tenocytes *in vitro* | 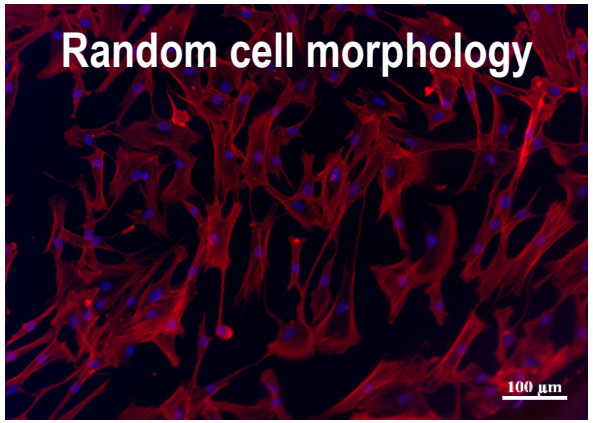 | 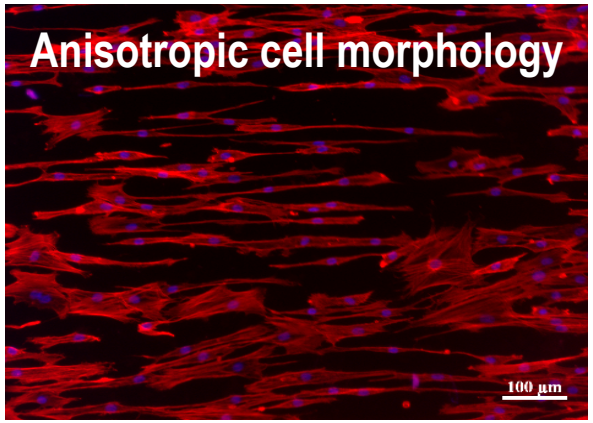 | 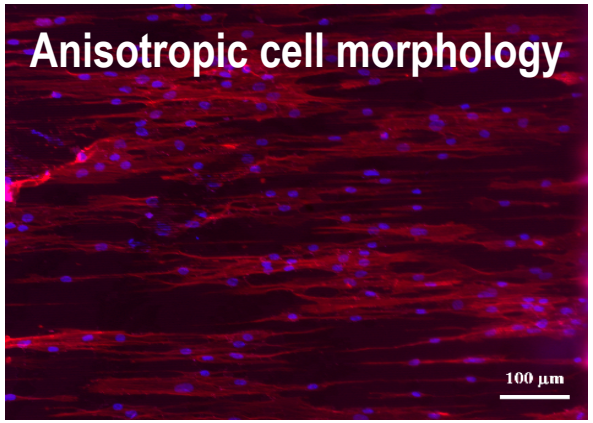 |
| Patellar tendon *in vivo* | 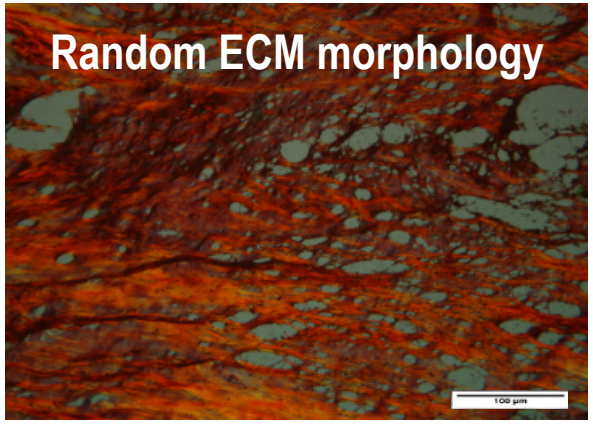 | 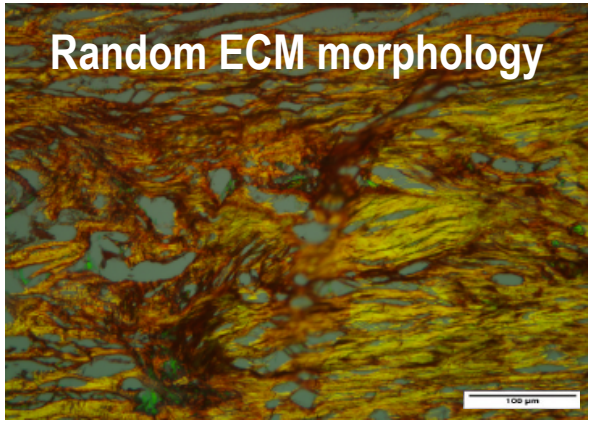 | 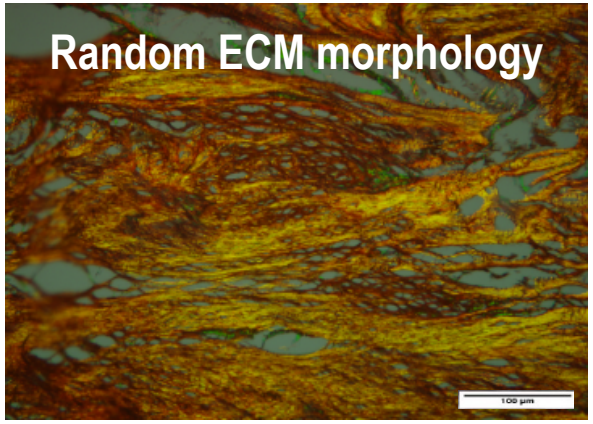 |
| Subcutaneous *in vivo* | 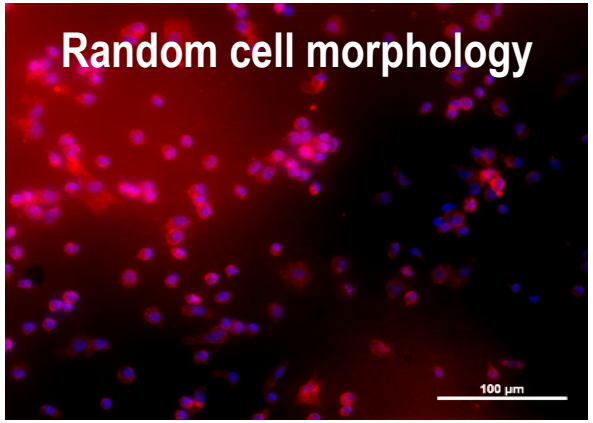 | 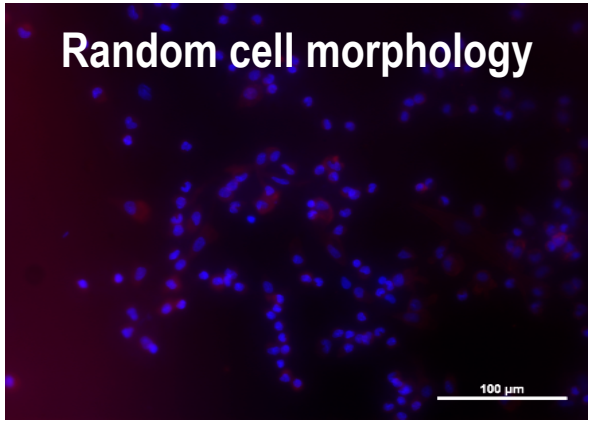 | 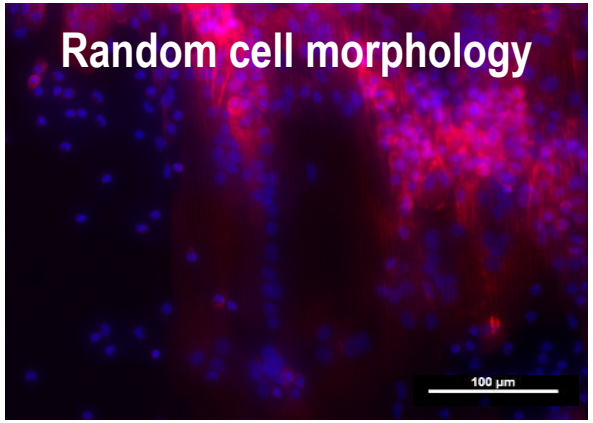 |